

Real-Time Adaptive Velocity Optimization for Autonomous Electric Cars at the Limits of Handling

Thomas Herrmann, Alexander Wischnewski, Leonhard Hermansdorfer, Johannes Betz, Markus Lienkamp

Abstract—With the evolution of self-driving cars, autonomous racing series like Roborace and the Indy Autonomous Challenge are rapidly attracting growing attention. Researchers participating in these competitions hope to subsequently transfer their developed functionality to passenger vehicles, in order to improve self-driving technology for reasons of safety, and due to environmental and social benefits. The race track has the advantage of being a safe environment where challenging situations for the algorithms are permanently created. To achieve minimum lap times on the race track, it is important to gather and process information about external influences including, e.g., the position of other cars and the friction potential between the road and the tires. Furthermore, the predicted behavior of the ego-car’s propulsion system is crucial for leveraging the available energy as efficiently as possible. In this paper, we therefore present an optimization-based velocity planner, mathematically formulated as a multi-parametric Sequential Quadratic Problem (mpSQP). This planner can handle a spatially and temporally varying friction coefficient, and transfer a race Energy Strategy (ES) to the road. It further handles the velocity-profile-generation task for performance and emergency trajectories in real time on the vehicle’s Electronic Control Unit (ECU).

Index Terms—Real-Time Numerical Optimization, Optimal Control, Velocity Planning, Trajectory Planning, Autonomous Electric Vehicles, Energy Strategy, Variable Friction Potential

I. INTRODUCTION

THE Technical University of Munich has been participating in the Roborace competition since 2018. Many parts of our software stack are already available on an open source basis [1] including the code of the algorithm in this work [2]. This paper explains an optimization-based Nonlinear Model Predictive Planner (NLMPP), mathematically formulated as a multi-parametric Sequential Quadratic Problem (mpSQP) [3], to calculate the velocity profiles during a race. The velocity planner inputs are the offered race paths (“performance” and “emergency”), stemming from our graph-based path-planning framework [4], see Fig. 1. The presented velocity optimization in combination with the path framework span our local trajectory planner that will be used within the competition. The trajectory planner’s output is forwarded to the underlying vehicle controller [5], [6], transforming the target trajectory into

T. Herrmann (corresponding author), L. Hermansdorfer, J. Betz and M. Lienkamp are with the Institute of Automotive Technology, Department of Mechanical Engineering, Technical University of Munich, Garching (Munich), 85748 Germany e-mail: thomas.herrmann@tum.de.

A. Wischnewski is with the Institute of Automatic Control, Department of Mechanical Engineering, Technical University of Munich, Garching (Munich), 85748 Germany

Manuscript received May 30, 2020; revised September 25, 2020; accepted December 24, 2020.

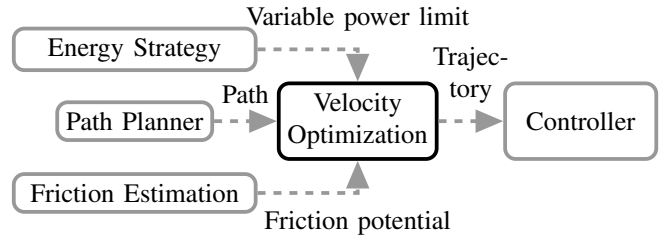


Fig. 1. Software environment of presented velocity optimization module.



Fig. 2. TUM Roborace DevBot 2.0 on the race track.

actuator commands for the race car, called “DevBot 2.0”, see Fig. 2. A huge motivation behind setting up an optimization-based velocity planner was to be able to handle information about the locally and temporally varying friction potential on the race track [7], and utilize the information provided by the race Energy Strategy (ES) [8] as a vehicle’s velocity profile has a significant influence on its energy consumption and power losses [9]. The friction potential estimation and the calculation of the ES are handled by separate modules in our software stack. Their outputs, the friction potential and variable power limits, are then considered in the presented velocity optimization algorithm.

To achieve real-time-capable calculation times, we build local approximations of the nonlinear velocity-planning problem, resulting in convex multi-parametric Quadratic Problems (mpQP) [10] that can be solved iteratively using a Sequential Quadratic Problem (SQP) method. We evaluated different open-source Quadratic Problem (QP) solvers and compared their solution qualities and calculation times to a direct solution of the Nonlinear Problem (NLP). We chose the Operator Splitting Quadratic Problem (OSQP) [11] solver as it outperformed its competitors on a standard x86-64 platform as well as on the DevBot’s automotive-grade Electronic Control Unit (ECU), the ARM-based NVIDIA Drive PX2.

A. State of the art

The field of trajectory planning of vehicles at the limits of handling is attracting growing attention in research. The scenarios where the car is required to be operated at the limits of its driving dynamics will become more and more important as we see the spread of cars equipped with self-driving functionality, and even fully autonomous vehicles. Through this, complex scenarios with self-driving vehicles on the road will occur more frequently. Research is also being carried out on the race track where these challenging scenarios can deliberately be created in a safe environment [12].

In the field of global trajectory optimization for race tracks, different mathematical concepts are applied. In the work of Ebbesen et al. [13] a Second Order Conic Problem (SOCP) formulation is used to calculate the optimal power distribution within the hybrid powertrain of a Formula One race car leading to globally time-optimal velocity profiles for a given path. For the same racing format, Limebeer and Perantoni [14] took into account the 3D geometry of the race track within their formulation of an Optimal Control Problem (OCP) to solve a Minimum Lap Time Problem (MTLP). In a similar approach, Tremlett and Limebeer [15] consider the thermodynamic effects of the tires. Christ et al. [16] consider spatially variable but temporally fixed friction coefficients along the race track to calculate time-optimal global race trajectories for a sophisticated Nonlinear Double Track Model (NDTM). They show a significant influence of the variable friction coefficients on the achievable lap time when considered during the trajectory optimization process. A minimum-curvature QP formulation, calculating the quasi-time-optimal trajectory for an autonomous race car on the basis of an occupancy grid map, is given by Heilmeyer et al. [5]. Their advantage in comparison to [16] is the computation time, but the resulting trajectories are suboptimal in terms of lap time. Also, Dal Bianco et al. [17] formulate an OCP to find the minimum lap time for a GP2 car and include a detailed multibody vehicle dynamics model with 14 degrees of freedom. However, none of these approaches are intended to work in real-time on a vehicle ECU, but to deliver detailed and close-to-reality results for lap time or for the sensitivity analysis of vehicle setup parameters.

A further necessary and important part in a software stack for autonomous driving is the online re-planning of trajectories to avoid static and dynamic obstacles at high speeds. The literature can be structured into the three fields:

- “separated/two-step trajectory planning”, where the velocity calculation is a subsequent process of the path planner [18]–[20].
- “combined trajectory planning”, optimizing both path and velocity at the same time [21]–[23].
- “Model Predictive Control (MPC) approaches” taking into account the current vehicle state [10], [24]–[27].

In the following, we evaluate the literature according to the implemented features regarding

- spatially and temporally varying friction coefficients,
- powertrain behavior,
- applicability at the limits of vehicle dynamics through fast computation times.

In the spline-based approach of Mercy et al. [23] trajectories for robots operating at low velocities are optimized. The calculation times of the general NLP-solver Interior Point OPTimizer (IPOPT) [28] range up to several hundred milliseconds, which is too long for race car applications. Another general NLP-formulation is done by Svensson et al. [29]. The latter describe a planning approach for safety trajectories of automated vehicles, which they validate experimentally in simulations for maximum velocities of 30 km h^{-1} , leveraging the general nonlinear optimal control toolkit ACADO [30].

Huang et al. [18] describe a two-step approach: first determining the path across discretized available space and then calculating a sufficient velocity. Also, Meng et al. [19] leverage a decoupled approach using a quadratic formulation for the speed profile optimization, reaching real-time capable calculation times below 0.1 s in this step. Nevertheless, both publications deal with low vehicle speeds in simulations of max. 60 km h^{-1} . Furthermore, Zhang et al. [20] implement a two-step algorithm where they use MTSOS [31] for the speed profile generation within several milliseconds for path lengths of up to 100 m. The speed-profile optimization framework MTSOS developed by Lipp and Boyd [31] works for fixed paths leveraging a change of variables. As in the aforementioned publications, they consider a static friction coefficient and neglect the maximum available power of the car. The same is true for the MPC algorithm by Carvalho et al. [24]. They plan trajectories considering the driving dynamics of a bicycle model, neglecting physical constraints stemming from the powertrain, like maximum available torque or power. This is a major drawback for our application, as the DevBot 2.0 is often operating at the power limit of its electric machines.

Subsits and Gerdes [21] formulate a Quadratically Constrained Quadratic Problem (QCQP) replanning path and velocity of a race car at spatially fixed points on the track to avoid static obstacles. They consider a constant friction potential and the maximum available vehicle power. However, the obstacles need to be known in advance before the journey commences, and must be placed at a decent distance from the replanning points to allow the algorithm to find a feasible passing trajectory, given the physical constraints. In order to reach fast calculation times, Alrifaae et al. [25] use a sequential linearization technique for real-time-capable trajectory optimization. They consider the friction maxima, with included velocity dependency that they determine beforehand. This dependency is assumed to be globally constant, thus neglecting the true track conditions during driving. Their experimental results stem from simulations with peak computation times of several hundred milliseconds on a desktop PC.

Considering variable friction on the road is attracting more attention, as it is an emergency-relevant feature for passenger cars and a performance-critical topic for race cars. Therefore, Svensson et al. [22] describe an adaptive trajectory-planning and optimization approach. They pre-sample trajectory primitives to avoid local optima in subsequent SQPs stemming mainly from avoidance maneuvers to the suboptimal side of an obstacle. The vehicle adaptively reacts to a varying friction potential on the road at speeds of up to 100 km h^{-1} . The resulting problem is solved using simulations in MATLAB,

so no information about the calculation speed on embedded hardware is given.

Stahl et al. [4] describe a two-step, multi-layered graph-based path planner. This approach allows for functionalities such as following other vehicles and overtaking maneuvers, also in non-convex scenarios at a high update rate. We use this path planner to generate the inputs for the velocity-optimization algorithm.

B. Contributions

In this paper we contribute to the state of the art in the field of real-time-capable trajectory planning with the following content.

(1) We formulate a tailored mpSQP algorithm capable of adaptive velocity planning for race cars operating at the limits of handling, and at velocities above 200 km h^{-1} . The planner computes velocity profiles for various paths using the path planner [4] in real time on the target hardware, an NVIDIA Drive PX2 [32] being an ECU already proven for autonomous driving. The adaptivity refers to the multi-parametric input to the planner, depending on the vehicle's environment. The quadratic subproblems within the mpSQP are handled using the OSQP [11] solver. Its primal and dual infeasibility detection for convex problems [33] was integrated to flag up (as fast as possible) offered paths which could not feasibly be driven [4].

(2) With the formulation of an mpSQP optimization algorithm, it is possible to integrate our race ES, described in our previous works [8], [34]. The necessary variable power parameters are forwarded to the velocity planner and considered as a hard constraint, see Fig. 1. In the case of electric race cars, such an ES is vital in order not to overstress the powertrain thermodynamically.

(3) We further allow the friction coefficient on the race track to vary spatially as well as temporally [7]. Therefore, global limits of the allowed longitudinal and lateral acceleration of the vehicle are omitted. This improves the achievable lap time significantly as the tires are locally exploited to their maximum. Via the temporal variation of the friction limits, we take into account varying grip due to, e.g., warming tires or changing weather conditions.

(4) To boost the solver selection for similar projects dealing with trajectory optimization within the community, we compare the efficiency of different solver types regarding calculation speed and solution quality. Therefore, we solve the quadratic subproblems in our mpSQP using a first-order Alternating Direction Method of Multipliers (ADMM) implemented in the OSQP-framework. Its results are compared to the active-set solver QP Online Active SEt Strategy (qpOASES) [35]. We contrast both SQPs with a direct solution of the nonlinear velocity optimization problem with the open-source, second-order interior point solver IPOPT [28], interfaced by the symbolic framework CasADi [36].

Section II introduces the mathematical background of an SQP method to solve an NLP. In the following Section III, the nonlinear equations of our velocity planner are introduced. We explain their efficient incorporation within an mpSQP and

explain details about the recursive feasibility of our optimization problem. The Results section shows the realization of the ES and the handling of variable friction by our velocity-optimization algorithm. Furthermore, we contrast different solvers in terms of their runtime and solution quality.

II. PRELIMINARIES

In this section, the mathematical background to an SQP optimization method to solve local approximations of an NLP with objective function $J(\mathbf{o})$, $h_b(\mathbf{o})$ and $g_c(\mathbf{o})$, denoting equality and inequality constraints of scalar quantity b and c , and optimization variables \mathbf{o} is introduced.

The standard form of a Nonlinear Optimal Control Problem (NOCP) is given by [36], [37]:

$$\min_{\mathbf{o}} J(\underbrace{x(s), u(s)}_{\mathbf{o}}) \quad (1)$$

$$\text{s.t. } \frac{dx(s)}{ds} = f(x(s), u(s)) \quad (2)$$

$$h_b(\mathbf{o}) = 0 \quad (3)$$

$$g_c(\mathbf{o}) \leq 0. \quad (4)$$

The independent space variable s describes the distance along the vehicle's path in our problem. The function $f(x(s), u(s))$ specifies the derivatives of the state variable $x(s)$ as a function of the state $x(s)$ and the control input $u(s)$.

The standard form of a QP is expressed as [38]

$$\begin{aligned} \min \quad & \frac{1}{2} \mathbf{z}_{\text{qp}}^T \mathbf{P} \mathbf{z}_{\text{qp}} + \mathbf{q}^T \mathbf{z}_{\text{qp}} \\ \text{s.t.} \quad & \mathbf{l} \leq \mathbf{A} \mathbf{z}_{\text{qp}} \leq \mathbf{u}, \end{aligned} \quad (5)$$

where \mathbf{z}_{qp} is the optimization vector, matrix \mathbf{P} is the Hessian matrix of the discretized objective $J(\mathbf{o}^k)$ and the vector \mathbf{q}^T equals the Jacobian of the discretized objective $\nabla J(\mathbf{o}^k)$ with iterate k . Matrix \mathbf{A} contains the linearized versions of the constraints h_b and g_c in the optimization problem. Their upper and lower bounds are summarized in both vectors, \mathbf{l} and \mathbf{u} .

In an SQP method, the linearization point \mathbf{o}^k is updated after every QP iteration k using [39]

$$\mathbf{o}^{k+1} = \mathbf{o}^k + \alpha \mathbf{z}_{\text{qp}} \quad (6)$$

$$\boldsymbol{\lambda}^{k+1} = \boldsymbol{\lambda}_{\text{qp}}^k \quad (7)$$

$$\mathbf{z}_{\text{qp}} = \mathbf{o} - \mathbf{o}^k. \quad (8)$$

In the quadratic subproblem, a solution for \mathbf{z}_{qp} is computed. We chose to initialize the Lagrange multiplier vector $\boldsymbol{\lambda}^{k+1}$ using the previous QP solution as stated in the local SQP algorithm in [40].

On the one hand, the steplength parameter α must be calculated in order to perform a large step in the direction of the optimum \mathbf{o}^* for fast convergence. On the other, α must be small enough to not skip or oscillate around \mathbf{o}^* . It is therefore necessary to define a suitable merit function, taking into account the minimization of the objective function as well as the adherence of the constraints [37], [39]. As it is hard to find such a merit function, we use the SQP Root Mean Square

Error (RMSE) $\bar{\varepsilon}_{\text{SQP}}$ as well as the SQP infinity norm error $\hat{\varepsilon}_{\text{SQP}}$ to determine whether a stepsize α is suitable or not,

$$\bar{\varepsilon}_{\text{SQP}} = \frac{1}{K} \|\mathbf{o}^{k+1} - \mathbf{o}^k\|_2 \leq \bar{\varepsilon}_{\text{SQP,tol}} \quad (9)$$

$$\hat{\varepsilon}_{\text{SQP}} = \|\mathbf{o}^{k+1} - \mathbf{o}^k\|_\infty \leq \hat{\varepsilon}_{\text{SQP,tol}}, \quad (10)$$

where K denotes the number of elements in \mathbf{o}^k . In case one of the two errors ε_{SQP} increases when applying (6), the counting variable γ is increased and, therefore, α is reduced until the tolerance criteria values $\bar{\varepsilon}_{\text{SQP,tol}}$ and $\hat{\varepsilon}_{\text{SQP,tol}}$ are met:

$$\alpha = \beta^\gamma. \quad (11)$$

The parameter $\beta \in]0, 1[$ is to be tuned problem-dependent as the Armijo rule states [37] with $\gamma \in [0; 1; 2; \dots]$.

To bring the objective $J(\mathbf{o})$ and the necessary nonlinear constraints $h_b(\mathbf{o})$ and $g_c(\mathbf{o})$ into the mathematical form of a QP (5), they are discretized and approximated quadratically or linearly, respectively, using Taylor series expansions in the form

$$J(\mathbf{o}) \approx \frac{1}{2}(\mathbf{o} - \mathbf{o}^k)^T \mathbf{P}(\mathbf{o}^k)(\mathbf{o} - \mathbf{o}^k) + \nabla J(\mathbf{o}^k)(\mathbf{o} - \mathbf{o}^k) + J(\mathbf{o}^k) \quad (12)$$

and

$$g_c(\mathbf{o}) \approx \nabla g(\mathbf{o}^k)(\mathbf{o} - \mathbf{o}^k) + g(\mathbf{o}^k). \quad (13)$$

III. OPTIMIZATION-BASED VELOCITY PLANNER

This section describes the implemented point mass model, the used objective function, and the constraints necessary to optimize the velocity on the available paths. The point mass model was chosen, as it is commonly used to describe the driving dynamics in the automotive context. Due to its simplicity, it delivers a small number of optimization variables and constraints. Therefore, quick solver runtimes can be achieved. It still delivers quite accurate results for the task of pure velocity optimization [13].

The concept of the optimization-based algorithm is to plan velocities with inputs from other software modules, cf. Section I. We do not deal with sensor noise in the planner but in the vehicle dynamics controller [5], which receives the trajectory input. The trajectory planning module, consisting of a path planner [4] and the presented velocity optimization algorithm, always keeps the first discretization points of a new trajectory constant with the solution from a previous planning step. After matching the current vehicle position to the closest coordinate in the previously planned trajectory, a new plan starting from this position is made within the remaining part of a new trajectory. Through this, two control loops can be omitted, and prevent from unnecessary inferences in the planning and the control module.

A. Nonlinear problem

This subsection presents the nonlinear velocity optimization problem, structured into its system dynamics, equality and inequality constraints as well as its objective function.

1) *System dynamics*: Let us first introduce the system dynamics of the point mass model for our physical vehicle state $v(s)$. Newton's second law for a point mass m_v states

$$m_v v(s) \frac{dv(s)}{ds} = m_v a_x(s). \quad (14)$$

With the derivative of the kinetic energy,

$$\frac{dE_{\text{kin}}(s)}{ds} = \frac{1}{2} m_v \frac{dv^2(s)}{ds} = m_v v(s) \frac{dv(s)}{ds}, \quad (15)$$

the system dynamics are given by the longitudinal acceleration

$$a_x(s) = \frac{1}{m_v} \frac{dE_{\text{kin}}(s)}{ds}. \quad (16)$$

The force $F_{x,p}(s)$ applied by the powertrain to move the point mass model can be calculated by

$$F_{x,p}(s) = m_v a_x(s) + c_r v^2(s) \quad (17)$$

where c_r is the product of the air density ρ_a , the air resistance coefficient c_w and the vehicle's frontal area A_v ,

$$c_r = \frac{1}{2} \rho_a c_w A_v. \quad (18)$$

2) *Equality and inequality constraints*: To improve numerical stability and avoid backward movement, the velocity $v(s)$ is constrained,

$$0 \leq v(s) \leq v_{\text{max}}(s). \quad (19)$$

To ensure that the optimization remains feasible in combination with a moving horizon, the terminal constraint

$$v(s_f) \leq v_{\text{end}} \quad (20)$$

on the last coordinate point s_f within the optimization horizon is leveraged. Here, v_{end} denotes the minimal velocity the vehicle can take in the case of maximum specified track curvature κ_{max} at the vehicle's technically maximum possible lateral acceleration $a_{y,\text{max}}$. Therefore,

$$v_{\text{end}} = \sqrt{\frac{a_{y,\text{max}}}{\kappa_{\text{max}}}}. \quad (21)$$

At the beginning of the optimization horizon, the velocity and acceleration must equal the vehicle's target states of the currently executed plan v_{ini} and $a_{x,\text{ini}}$,

$$v(s_s) = v_{\text{ini}}, \quad a_{x,\text{ini}} - \delta_a \leq a_x(s_s) \leq a_{x,\text{ini}} + \delta_a, \quad (22)$$

where s_s denotes the first coordinate within the moving optimization horizon and δ_a a small tolerance to account for numerical imprecision.

As the vehicle's maximum braking as well as driving forces are technically limited, the resulting constraints are

$$F_{\text{min}} \leq F_{x,p}(s) \leq F_{\text{max}}. \quad (23)$$

The negative force constraint F_{min} does not affect the optimization-problem feasibility, as the DevBot's braking actuators can produce more negative force than the tires can transform.

The electric machine's output power $P(s)$ is computed using

$$P(s) = F_{x,p}(s)v(s), \quad (24)$$

limited by the available maximum

$$P(s) \leq P_{\max}(s). \quad (25)$$

We highlight that $P_{\max}(s)$ is a space-dependent parameter in contrast to the constant maximum force F_{\max} . By this, the given race ES based on our previous works [8], [34] is realized.

To further integrate the tire physics, we interpret the friction potential as a combined, diamond-shaped acceleration limit for the vehicle [7] given by the inequality

$$\|(\hat{a}_x(s), \hat{a}_y(s))\|_1 \leq 1 + \epsilon(s) \quad (26)$$

where $\|\cdot\|_1$ denotes the l^1 -norm. Furthermore, the normalized longitudinal $\hat{a}_x(s)$ as well as the lateral tire utilizations $\hat{a}_y(s)$ are given by

$$\hat{a}_x(s) = \frac{F_{x,p}(s)}{m_v} \frac{1}{\bar{a}_x(s)}, \quad \hat{a}_y(s) = \frac{a_y(s)}{\bar{a}_y(s)}. \quad (27)$$

Here, we use $\bar{a}_{x/y}(s)$ to indicate a variable, space-dependent acceleration potential in both longitudinal and lateral direction, which is to be leveraged [7]. The lateral acceleration $a_y(s)$ reads [41]

$$a_y(s) = \kappa(s)v^2(s) \quad (28)$$

accounting for the target path geometry by the variable road curvature parameter $\kappa(s)$.

In (26) the slack variable $\epsilon(s)$ ensures the recursive feasibility of the optimization problem: details are given in Subsection III-D. We constrain the slack variable $\epsilon(s)$ by

$$0 \leq \epsilon(s) \leq \epsilon_{\max} \quad (29)$$

to prohibit negative values and additionally keep the physical tire exploitation within a specified maximum.

Similarly to (21), the longitudinal and lateral acceleration limits at the end of the optimization horizon $\bar{a}_x(s_f)$ and $\bar{a}_y(s_f)$ must be set to the lowest physically possible acceleration limits $\bar{a}_{x/y,\min}$ for the current track conditions,

$$\bar{a}_{x/y}(s_f) \leq \bar{a}_{x/y,\min}. \quad (30)$$

3) *Continuous objective function:* With the help of the introduced symbols and equations we can now formulate the objective function $J(x(s))$ to minimize the traveling time along the given path:

$$J(x(s)) = \int_0^{s_f} \frac{1}{v(s)} ds + \frac{\rho_j}{s_f} \int_0^{s_f} \left(\frac{d^2 v(s)}{dt^2} \right)^2 ds + \frac{\rho_{\epsilon,1}}{s_f} \int_0^{s_f} \epsilon(s) ds + \frac{\rho_{\epsilon,q}}{s_f} \int_0^{s_f} \epsilon^2(s) ds. \quad (31)$$

We chose the optimization variables \mathbf{o} to be the state velocity $v(s)$ as well as the slacks $\epsilon(s)$. The control input to the vehicle $u(s) = F_{x,p}(s)$ doesn't occur explicitly in the objective function but can be recalculated from the state trajectory $v(s)$, cf. (17).

Minimizing the term $\frac{1}{v(s)}$ is equivalent to the minimization of the lethargy $\frac{dt}{ds}$, which can be interpreted as the time necessary to drive a unit distance [13]. To weight the different terms, the penalty parameters ρ are used. These include a jerk penalty ρ_j , a slack weight $\rho_{\epsilon,1}$ on their integral and a penalty

$\rho_{\epsilon,q}$ on the integral of the squared slack values. The linear penalty term on the slack variable $\epsilon(s)$ is necessary to achieve an exact penalty maintaining the original problem's optimum $[v^*(s) \ \epsilon^*(s)]$ if feasible [42]. Similar to a regularization term, the integral of the squared slacks $\epsilon(s)$ is additionally added to improve numerical stability and the smoothness of the results.

B. Multi-parametric Sequential Quadratic Problem

This chapter gives details about the implementation of the NLP given in Subsection III-A as an mpSQP in order to efficiently solve local approximations of the velocity planning problem. We describe how to approximate the nonlinear objective function $J(x(s))$ (31) to achieve a constant and tuneable Hessian matrix within our tailored mpSQP algorithm. Furthermore, we present a method to reduce the number of slack variables $\epsilon(s)$ and the slack constraints (29) therefore necessary.

Our optimization vector $\mathbf{z} = \mathbf{o}^k$ in a discrete formulation transforms into

$$\mathbf{z} = \left[\underbrace{v_1(s_1) \dots v_{M-1}(s_{M-1})}_{\mathbf{v}} \quad \underbrace{\epsilon_0(s_0) \dots \epsilon_{N-1}(s_{N-1})}_{\boldsymbol{\epsilon}} \right]^T \in \mathbb{R}^{K \times 1} \quad (32)$$

where $K = M - 1 + N$ where M denotes the number of discrete velocity points v_m and N the number of discrete slack variables ϵ_n used in the tire inequality constraints within one optimization horizon. We drop the dependency of \mathbf{z} on s_m in the following for the sake of readability. The velocity variable v_0 is removed from the vector \mathbf{z} as it is a fixed parameter equaling the velocity planned in a previous SQP $l - 1$ for the current position.

To reduce the problem size, we apply one slack variable ϵ_n to multiple consecutive discrete velocity points v_m . This is done uniformly and leads to:

$$\left[\underbrace{v_1 \dots v_{\tilde{N}}}_{\epsilon_0} \quad \underbrace{v_{\tilde{N}+1} \dots v_{2\tilde{N}}}_{\epsilon_1} \quad \underbrace{v_{2\tilde{N}+1} \dots v_{M-1}}_{\dots} \right] \quad (33)$$

Here, \tilde{N} is a problem-specific parameter setting a trade off between the number of optimization variables and therefore the calculation speed and accuracy in the solution.

From domain knowledge we know that the objective function can be approximated in the form

$$J(\mathbf{z}) \approx \underbrace{\|\mathbf{v} - \mathbf{v}_{\max}\|_2^2}_{J_v} + \underbrace{\rho_j \|\Delta \mathbf{v}\|_2^2}_{J_j} + \underbrace{\rho_{\epsilon,1} \|\zeta \boldsymbol{\epsilon}\|_1^2}_{J_{\epsilon,1}} + \underbrace{\rho_{\epsilon,q} \|\zeta \boldsymbol{\epsilon}\|_2^2}_{J_{\epsilon,q}}. \quad (34)$$

The slack variables are transformed via the constant factor ζ ; how this is selected is discussed at the end of this section. By using the l^2 -norm of the vector difference of \mathbf{v} and \mathbf{v}_{\max} , the solution tends to minimize the travel time along the path. Still, this formulation in combination with (19) makes the car keep a specified maximum velocity $v_{\max}(s)$ dependent on the current position s to react, e.g., to other cars. To control the

vehicle's jerk behavior, we add the Tikhonov regularization term $\rho_j \|\Delta \mathbf{v}\|_2^2$ [38] that approximates the second derivative of \mathbf{v} . The tridiagonal Toeplitz matrix $\Delta \in \mathbb{R}^{M-3 \times M-1}$ contains the diagonal elements $(1 \ -2 \ 1)$ [38]. By the l^1 -norm within $J_{\epsilon,1}$, the summation of the absolute values of the slack variable vector entries in ϵ is achieved. To improve the numerical conditioning of the problem, their l^2 -norm is added additionally by $J_{\epsilon,q}$.

For the specific choice of cost function in (12), the Hessian matrix $\mathbf{P} \in \mathbb{R}^{K \times K}$ does not depend on \mathbf{z} . The condition number $\sigma_{\mathbf{H}}$ of the Hessian \mathbf{P} is tuned to be as close to 1 as possible via the penalties ρ_j and $\rho_{\epsilon,1}$ as well as ζ denoting the unit conversion factor of the tire slack variable values in ϵ to SI units:

$$\mathbf{P} = \left[\begin{array}{ccc|cc} \ddots & \ddots & 0 & & \\ \ddots & c_j \rho_j & \ddots & & 0 \\ 0 & \ddots & \ddots & & \\ \hline & 0 & & 2\rho_{\epsilon,q} \zeta^2 & 0 \\ & & & 0 & \ddots \end{array} \right] \quad (35)$$

The function $c_j \rho_j$ represents different constant entries j that are linearly dependent on ρ_j . This upper left part of \mathbf{P} is a bisymmetric matrix with constant entries on its main diagonal, as well as on its first and second ones.

By using the approach of multi-parametric programming, we can vary several problem parameters online in the SQP (Section II) without changing the problem size. These parameters include the

- spatial discretization length Δs_m .
- curvature of the local path $\kappa(s_m)$ [4].
- maximum allowed velocity $v_{\max}(s_m)$.
- power limitations $P_{\max}(s_m)$ stemming from a global race strategy taking energy limitations into account [8], [34].
- longitudinal and lateral acceleration limits $\bar{a}_x(s_m)$, $\bar{a}_y(s_m)$ [7].

C. Variable acceleration limits

To fully utilize the maximum possible tire forces, a time- and location-dependent map of the race track, containing the maximum possible accelerations, is generated. The acceleration limits can be interpreted as vehicle-related friction coefficients, cf. Subsection III-A. The 1D map along the global coordinate s_{glo} with variable discretization step length stores the individual acceleration limitations $\Sigma_{\bar{a}}(s_{\text{glo}})$ in longitudinal and lateral directions. The acceleration limits are used in the selected local path as the parameters $\bar{a}_{x/y}(s)$ (27). It is important to know that while the vehicle proceeds, the target path is updated constantly, i.e., the global coordinates s_{glo} selected as the local path s vary permanently in subsequent velocity optimizations. The path planning guarantees to reuse the first few global coordinates s_{glo} from a previous timestep t^0 as the starting coordinates s_m of the subsequently chosen path at t^1 . Still, the path coordinates s_m at the end of the planning horizon are not guaranteed to precisely match all of the previously used global coordinates s_{glo} since the

path might change. Therefore, the requested coordinates in the acceleration map do also vary slightly, but are matched to the same local coordinate indices in s_m within the local path in subsequent timesteps. This leads to differences in the acceleration limits $\bar{a}_{x/y}(s_m)$ in subsequent planning iterations for identical local path indices m and therefore probably to infeasible problems in terms of optimization, see Section III-D.

The nature of the discretization problem is illustrated in Fig. 3. The given example provides stored acceleration limits $\Sigma_{\bar{a}}(s_{\text{glo}})$ in 10 m steps. The planning horizon ranges from $s_{\text{glo}} = 0$ m to 300 m. Therefore, we show a snippet of the end of the planning horizon ($s_{\text{glo}} = 200$ m to 270 m) as the discretization issues are clearly visible here. At timestep t^0 , the planning algorithm requests the stored acceleration limits $\Sigma_{\bar{a}}(s_{\text{glo}})$ every 5.5 m, starting at $s_{\text{glo}} = 0$ m. Within the depicted path snippet, the subsequent iteration at t^1 starts at a shift of 2.0 m with the same stepsize.

The simple approach of directly obtaining the local acceleration limits from the stored values $\Sigma_{\bar{a}}(s_{\text{glo}})$ by applying zero-order hold comes with drawbacks. A slight shift in the global coordinate selection can lead to situations where the acceleration limits $\bar{a}_{x/y}(s_m)$ differ between subsequent timesteps (t^0 , t^1) in the local path. If the subsequent acceleration limits $\bar{a}_{x/y}(s_m)$ at t^1 are smaller, they can lead to infeasibility. In Fig. 3, the gray areas highlight the situations where the obtained acceleration limits $\bar{a}_{x/y}(s_m)$ at t^1 are smaller compared to t^0 for identical local path indices m .

To mitigate the discretization effects, we propose an interpolation scheme leading to the values $\tilde{\Sigma}_{\bar{a}}(s_{\text{glo}})$. It applies linear interpolation between the stored acceleration limits $\Sigma_{\bar{a}}(s_{\text{glo}})$ but acts cautiously in the sense that it always underestimates the actual values $\Sigma_{\bar{a}}(s_{\text{glo}})$. This can be seen from $s_{\text{glo}} = 200$ m to 210 m, where the value is kept constant instead of interpolating between 11 and 12 m s^{-2} , and from $s_{\text{glo}} = 230$ m to 240 m where the algorithm adapts to the decreasing values although the stored value is 13 m s^{-2} . Then, zero-order hold is applied to this conservatively interpolated line. The limits obtained at t^1 often lie above $\bar{a}_{x/y}(s_m)$ at t^0 , which allow higher accelerations $a_{x/y}(s_m)$ than expected at t^0 and thus compensating for overestimated areas (gray areas).

The acceleration limits $\Sigma_{\bar{a}}(s_{\text{glo}})$ are constantly updated by an estimation algorithm [7] and are therefore also considered time-variant. During the update process, it must be guaranteed that the update does not lead to an infeasible vehicle state for the velocity-planning algorithm, e.g., when the vehicle is approaching a turn already utilizing full tire forces under braking, and the acceleration limits are suddenly decreased in front of the vehicle. Therefore, the updates only take place outside the planning horizon of the algorithm.

The difference between subsequently obtained acceleration limits $\bar{a}_{x/y}(s_m)$ at identical local path coordinates s_m can be controlled via the maximum change between the stored values $\Sigma_{\bar{a}}(s_{\text{glo}})$. The slope of the interpolated values $\tilde{\Sigma}_{\bar{a}}(s_{\text{glo}})$ can be used to calculate the maximum error when applying a particular step size Δs_m in path planning.

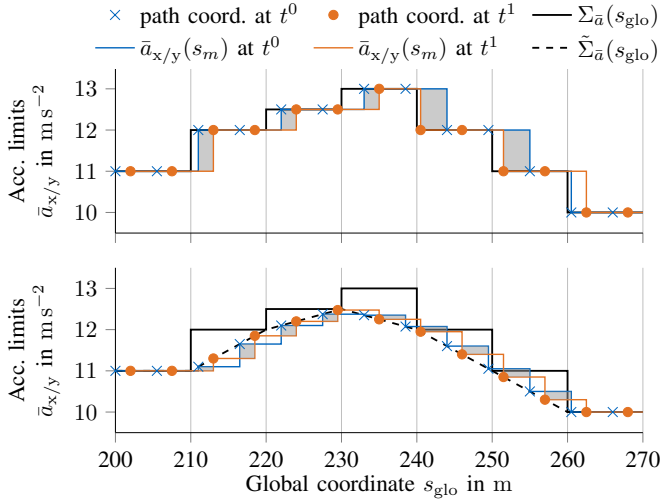


Fig. 3. Diagram of acceleration limits for two subsequently planned paths; with pure readout values $\Sigma_{\bar{a}}(s_{\text{glo}})$ (top) and with the proposed interpolation scheme $\tilde{\Sigma}_{\bar{a}}(s_{\text{glo}})$ (bottom). Gray areas show where the subsequently planned path receives decreased maximum acceleration limits $\bar{a}_{x/y}(s_m)$ due to tolerances in the spatial discretization.

D. Recursive feasibility

The minimum-time optimization problem tends to produce solutions with many active constraints, as it maximizes the tire utilization. It follows from this property, that ensuring recursive feasibility is a highly relevant aspect for the application of such an algorithm, and should be achieved via the terminal constraints (21) and (30) by making a worst-case assumption about the curvature $\kappa(s_f)$ and acceleration limits $\bar{a}_{x/y}(s_f)$ at the end of the optimization horizon. This property holds as long as the optimization problem is shifted by an integer multiple of the discretization Δs_m while the relations of the local path coordinates s_m with the curvature $\kappa(s_m)$ and the acceleration limits $\bar{a}_x(s_m)$ and $\bar{a}_y(s_m)$ remain constant. This cannot be ensured since the path planner [4] might slightly vary the target path due to an obstacle entering the planning horizon, or due to discretization effects. This leads to a deviation in the curvature profile $\kappa(s_m)$ and deviations in the admissible accelerations $\bar{a}_x(s_m)$ and $\bar{a}_y(s_m)$ since the local coordinate s_m might refer to a different point in global coordinates s_{glo} now, see Fig. 3.

To mitigate this deficiency, we introduce slack variables ϵ based on the exact penalty function approach [42]. This strategy ensures that the hard-constrained solution is recovered if it is feasible, and therefore the solution is not altered by addition of the slacks unless it is mandatory. The nature of the combined acceleration constraint (26) allows for a straightforward interpretation of the slack variables as a violation of ϵ in %. Together with the upper bound on the slack variables in (29), we can therefore state that the optimization problem is always feasible as long as the maximum required violation is limited to ϵ_{max} . In case no solution is found within the specified tolerance band, a dedicated failure-handling strategy is employed within the trajectory planning framework. We wish to point out that a suitable scaling of the slack variables is crucial to achieve sufficiently tight tolerances $\epsilon_{\text{QP,tol}}$ when

TABLE I
EMERGENCY- AND PERFORMANCE-SQP PARAMETRIZATION.

| Parameter | Unit | Value | |
|-----------------------------------|----------------------------|-------------|-----------|
| | | Performance | Emergency |
| M | - | 115 | 50 |
| N | - | 12 | 5 |
| δ_a | m s^{-2} | 0.1 | inactive |
| ϵ_{max} | % | 3.0 | 3.0 |
| ρ_j | - | $3e^2$ | 0.0 |
| $\rho_{\epsilon,1}$ | $\text{m}^2 \text{s}^{-2}$ | $1e^5$ | $5e^4$ |
| $\rho_{\epsilon,q}$ | $\text{m}^2 \text{s}^{-2}$ | $1e^4$ | $1e^3$ |
| $n_{\text{SQP,max}}$ | - | 20 | 20 |
| Δt_{max} | ms | 300 | 100 |
| β | - | 0.5 | 0.5 |
| $\bar{\epsilon}_{\text{SQP,tol}}$ | - | $1e^0$ | $1.5e^0$ |
| $\hat{\epsilon}_{\text{SQP,tol}}$ | - | $1e^0$ | $1.5e^0$ |
| $\epsilon_{\text{QP,tol}}$ | - | $1e^{-2}$ | $1e^{-2}$ |

using a numerical QP solver. We therefore employ a variable transformation with $\epsilon = \zeta \epsilon_n$ and optimize over ϵ_n instead. Realistic values for the maximum slack variable ϵ_{max} were found to be around 3% in extensive simulations on different race tracks (Berlin (Germany), Hong Kong (China), Indianapolis Motor Speedway (USA), Las Vegas Motor Speedway (USA), Millbrook (UK), Modena (Italy), Monteblanco (Spain), Paris (France), Upper Heyford (UK), Zalazone (Hungary)) and obstacle scenarios. We consider this to be an acceptable tolerance level and believe it will be difficult to achieve significantly tighter guarantees in the face of the scenario complexity we tackle in [4].

IV. RESULTS

In this section, the results achieved with the presented velocity mpSQP will be presented. We conducted the experiments on our Hardware-in-the-Loop simulator, which consists of a Speedgoat Performance real-time target machine, where validated physics models of the real race car in combination with realistic sensor noise are implemented. An additional NVIDIA Drive PX2 receives this sensor feedback and calculates the local trajectories. A Speedgoat Mobile real-time target machine transforms this trajectory input into low level vehicle commands to close the loop to the physics simulation. Therefore, we used the DevBot 2.0 data: $m_v = 1160 \text{ kg}$, $P_{\text{max}} = 270 \text{ kW}$, $F_{\text{max}} = 7.1 \text{ kN}$, $F_{\text{min}} = -20 \text{ kN}$, $c_r = 0.85 \text{ kg m}^{-1}$. The results in this section have been produced with the velocity planner parametrizations given in Table I.

We show results for two types of offered paths: performance and emergency. The emergency path is identical to the performance one, except for a coarser spatial discretization, and the fact that the velocity planner tries to stop as soon as possible on the emergency line. The optimization of the emergency line requires therefore fewer variables $M + N$. This formulation reduces the necessary calculation time of the emergency line that must be updated more frequently for safety reasons.

A. Objective function design

To explain the chosen values of the penalty weights ρ , we show the values of the single objective function terms in $J(\mathbf{z})$

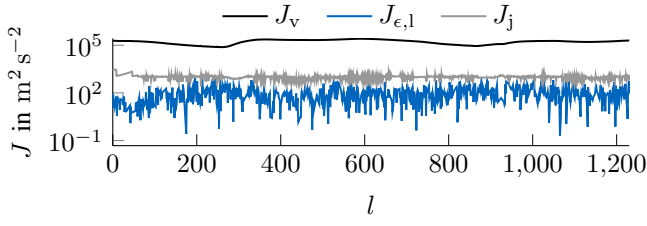


Fig. 4. Cost terms of the objective function J being minimized within the performance velocity profile. J_v shows the most significant influence on the solution due to its value range compared to the other objective terms J_j , $J_{\epsilon,1}$ and $J_{\epsilon,q}$ (not displayed as it equals almost 0). Symbol l denotes the number of the optimized velocity profiles.

being minimized during the calculation of the performance velocity profile in Fig. 4. The symbol l denotes the number of the optimized velocity profiles during the driven lap (including the race start) as well as the vehicle's stopping scenario. It can clearly be seen that the velocity term J_v has the highest relative impact on the optimum solution. Its value range is at least two orders of magnitude higher than the slack penalty terms $J_{\epsilon,1}$, $J_{\epsilon,q}$ (not displayed) and the jerk penalty J_j . The penalty weight $\rho_{\epsilon,1}$ on the linear slack term was chosen to increase the value of $J_{\epsilon,1}$ to be one order of magnitude higher than J_v if ϵ_{\max} was fully exploited on all the slack variables ϵ_n . Therefore, $J_{\epsilon,1}$ prevents the solver from permanent usage of tire slack ϵ for further lap time gains. As $\rho_{\epsilon,q}$ is applied to the squared values ϵ_n , it is sufficient to keep the magnitude of $\rho_{\epsilon,q}$ one order smaller than $\rho_{\epsilon,1}$. To provide a smooth velocity profile, we set the jerk penalty ρ_j to increase the value of J_j to be higher than the slack penalty terms during normal operation. By this, effects on a possible lap time loss stay as small as possible, whilst a smoothing effect in the range of numerical oscillations on the velocity and acceleration profile is still visible.

We further integrated a calculation time limit Δt_{\max} for the velocity optimization and a maximum SQP iteration number $n_{\text{SQP,max}}$. In case of reached limits, the algorithm would return the last suboptimal but driveable solution. The SQP never reached these limits during our experiments, and they can be considered as safety limitations. Instead, the SQP-algorithm always terminated due to the reached tolerance criteria $\bar{\epsilon}_{\text{SQP,toI}}$ and $\hat{\epsilon}_{\text{SQP,toI}}$, cf. (9) and (10).

B. Energy Strategy

As stated in Subsection III-B, the presented mpSQP is able to implement our global race ES [8], [34]. The ES is pre-computed offline and re-calculated online due to disturbances, unforeseen events during the race and model uncertainties. Through this, we account for the limited amount of stored battery energy and the thermodynamic limitations of the electric powertrain. Therefore, the ES delivers the maximum permissible power $P_{\max}(s_{\text{glo}})$ in order to reach the minimum race time, see Fig. 1. It takes the following effects into account:

- the vehicle dynamics in the form of an NDTM including a nonlinear tire model;

- the electric behavior of battery, power inverters and electric machines, i.e., the power losses of these components during operation;
- the thermodynamics within the powertrain transforming power losses into temperature contribution.

Fig. 5 depicts the output of the ES computed offline (top). We varied the amount of energy available for one race lap by the three values 100 % ($E_{\text{glo},100}(s_{\text{glo}})$), 80 % ($E_{\text{glo},80}(s_{\text{glo}})$) and 60 % ($E_{\text{glo},60}(s_{\text{glo}})$). The optimal power usage $P_{\text{glo}}(s_{\text{glo}})$ belonging to these energy values $E_{\text{glo}}(s_{\text{glo}})$ is depicted in the first diagram. The positive values in $P_{\text{glo}}(s_{\text{glo}})$ become the parametric input of the power constraint within the velocity optimization (25). By this formulation, we only restrict the vehicle's acceleration power but leave the braking force unaffected. This experiment consists of one race lap with constant maximum acceleration values $\bar{a}_{x/y}$ on the Modena (Italy) race circuit.

The power usage $P_{\text{loc},80}(s_{\text{glo}})$ locally planned by the mpSQP is shown in the middle plot of Fig. 5. The positive power values in $P_{\text{loc},80}(s_{\text{glo}})$ remained below the maximum power request allowed by the global strategy $P_{\text{glo},80}(s_{\text{glo}})$. Differences between the globally optimal power usage $P_{\text{glo}}(s_{\text{glo}})$ and the locally transformed power $P_{\text{loc}}(s_{\text{glo}})$ stem from different model equations in both - offline ES and online mpSQP - optimization algorithms. The velocity planner's point mass is more limited in its combined acceleration potential due to the diamond-shaped acceleration constraint (26) compared to the vehicle dynamics model (NDTM) in the ES. The NDTM overshoots the dynamical capability of the car slightly in edge cases due to parameter-tuning difficulties. Furthermore, the effect of longitudinal wheel-load transfer is considered within the NDTM. For these reasons, the point mass model accelerates less but meets the maximum admissible power $P_{\text{glo}}(s_{\text{glo}})$ on the straights. The accumulated error in this experiment can be expressed by the energy demand E_{loc} resulting from

$$E_{\text{loc}} = \int F_{x,p}(s_{\text{glo}}) ds_{\text{glo}}. \quad (36)$$

In total, an energy amount of $E_{\text{glo}} = 1.27 \text{ kWh}$ was allowed whereas $E_{\text{loc}} = 1.07 \text{ kWh}$ was used, implying 15.8 % drift. With the help of a re-calculation strategy adjusting the ES during the race, this error can be significantly reduced. This feature was switched off during this experiment to isolate the working principle of the race ES, i.e., the interaction between global and local planners.

The effect of the ES on the vehicle speed v_{P80} is depicted in Fig. 6. The left part (A) of both plots consists of a scenario where the race car is accelerating with the maximum available machine power of $P_{\max} = 270 \text{ kW}$ and a subsequent straight where the ES forces the vehicle to coast ($P_{\text{glo},80}(s_m) = P_{\text{loc},80}(s_m) = 0 \text{ kW}$). Acceleration without any power restriction on this straight would have resulted in the velocity curve v_{P100} meaning a slightly higher top speed by approx. 4 % or 8 km h^{-1} . The second part (B) of the shown planning horizon ensures recursive feasibility. Here, we force the velocity variable $v(s_N)$ to reach v_{end} (20).

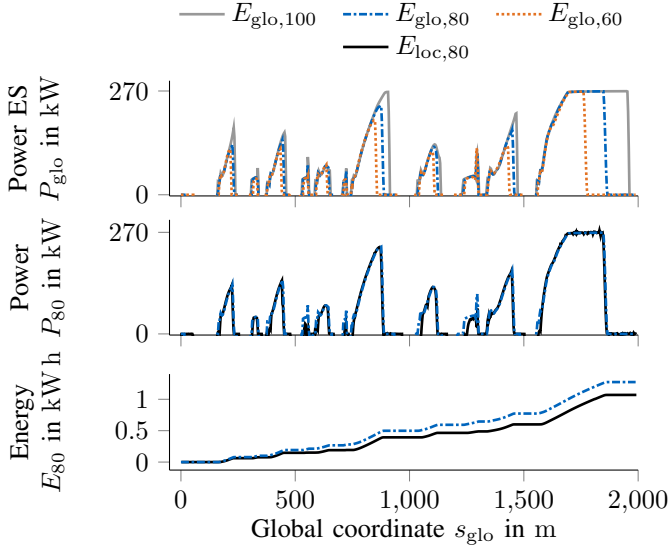


Fig. 5. Top: Optimal power usage $P_{glo}(s_{glo})$ from the ES that should be requested whilst driving on the Modena (Italy) race track. Mid: Power planned locally $P_{loc,80}(s_{glo})$ compared to $P_{glo,80}(s_{glo})$ resulting in an absolute drift in the energy demand between $E_{glo,80}(s_{glo})$ and $E_{loc,80}(s_{glo})$ of approx. 15.8% within one race lap (bottom).

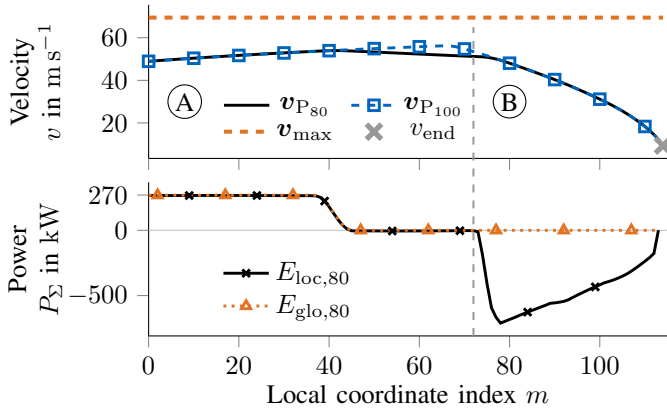


Fig. 6. The effect of the ES on one solution of the velocity-planning problem on the vehicle speed v_{P80} . In part (A), the race car is accelerating with the maximum available machine power of $P_{\Sigma} = 270$ kW and is forced to coast ($P_{glo}(s_m) = P_{loc}(s_m) = 0$ kW) thereafter. Acceleration without any power restriction is denoted by v_{P100} . Part (B) of the planning horizon ensures recursive feasibility.

C. Variable acceleration limits

Fig. 7 shows a locally variable acceleration map to determine the values of $\bar{a}_y(s)$ along the driven path. We conducted three experiments with a constant acceleration potential of $\bar{a}_x = 12.5 \text{ m s}^{-2}$ and varied \bar{a}_y in three different ways:

- $\bar{a}_{y,cst}^+$ has a constant value of 12.5 m s^{-2} along the entire track, describing a high friction potential.
- $\bar{a}_{y,cst}^-$ has a constant value of 6.5 m s^{-2} along the entire track, describing a low friction potential.
- $\bar{a}_{y,var}(s)$ has a variable value in the range of 6.5 m s^{-2} to 12.5 m s^{-2} with the steepest gradients between $s_{glo} = 1520 - 1550 \text{ m}$ and $s_{glo} = 1670 - 1700 \text{ m}$, as shown in Fig. 7.

The results of these experiments can be seen in Fig. 8. We

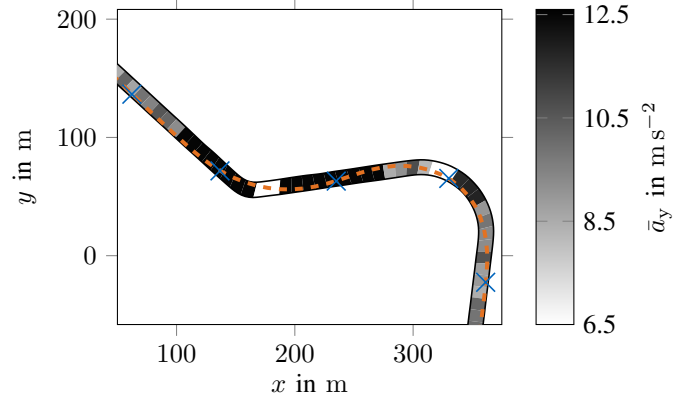


Fig. 7. Race track map displaying the spatially variable acceleration potential $\Sigma \bar{a}(s_{glo})$ including the driven path and markers starting from the global s -coordinate of 1400 m at 100 m gaps.

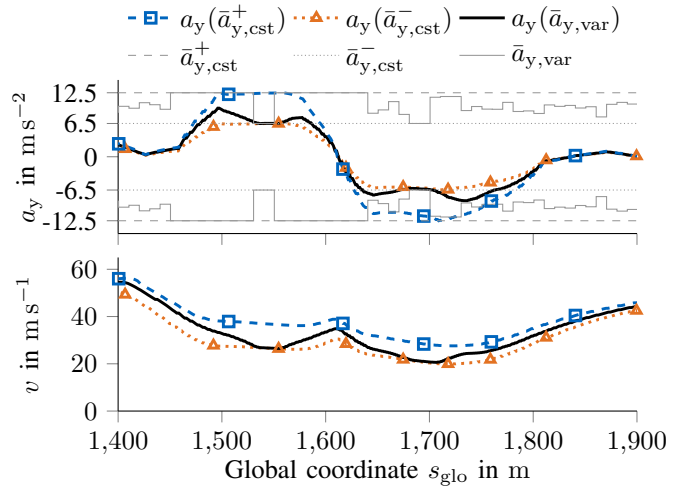


Fig. 8. Comparison of velocity $v(s_{glo})$ and lateral acceleration $a_y(s_{glo})$ profiles resulting from spatially and temporally varying acceleration coefficients $\bar{a}_y(s_{glo})$.

depicted the acceleration potentials \bar{a}_y of the three scenarios in combination with the planned lateral acceleration $a_y(s_{glo})$ (top) and the vehicle velocity $v(s_{glo})$ (bottom). In both scenarios with constant $\bar{a}_{y,cst}$ values, the planner leverages the entire admissible lateral potentials which can be seen between $s_{glo} = 1500 - 1600 \text{ m}$ and $s_{glo} = 1650 - 1700 \text{ m}$. The results achieved using the variable $\bar{a}_{y,var}(s)$ are interesting: The planned lateral acceleration $a_y(s)$ stayed within the boundaries of the low- and high-friction experiments. The planner handles the drop of $\bar{a}_{y,var}(s)$ of 50% at $s_{glo} = 1520 \text{ m}$ by reducing $a_y(s)$ in advance, while still fully leveraging $\bar{a}_{y,var}(s)$. This results in a vehicle velocity of $v(s_{glo})$ in the low-friction scenario. The same is true for $s_{glo} = 1670 \text{ m}$. Also during the rest of the shown experiment, the oscillating values of $\bar{a}_{y,var}(s)$ can be handled by the mpSQP algorithm. This behavior allows us to fully exploit the dynamical limits of the race car on a track with variable acceleration potential.

A further indicator that the velocity planner utilizes the full acceleration potential is shown in Fig. 9. Here, we depicted the

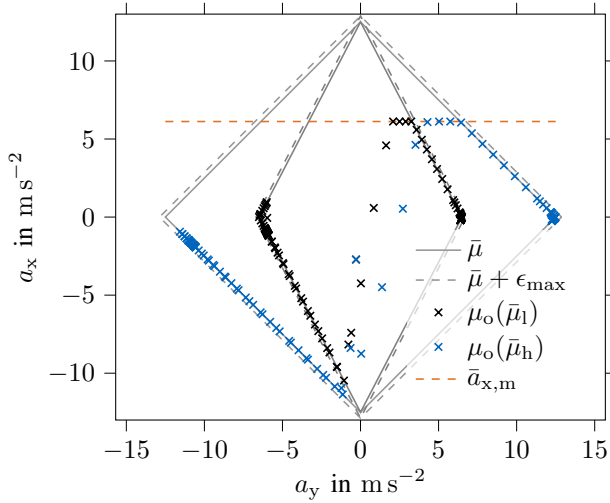


Fig. 9. Acceleration limit model including operating points at low- and high-friction experiments ($\bar{\mu}_l$ and $\bar{\mu}_h$) for a planning horizon ranging from the global coordinate of $s_{\text{glo}} = 1500$ m to 1800 m.

vehicle's optimized operating points $\mu_o(s)$ regarding combined acceleration $a_x(s)$ and $a_y(s)$ within the planning horizon of $s_{\text{glo}} = 1500 - 1800$ m. Both solid diamond shapes express the given constant acceleration limits of the high-friction scenario, $\bar{\mu}_h = \bar{a}_x$ & $\bar{a}_{y,\text{cst}}^+ = 12.5$ & 12.5 m s^{-2} , and the low-friction scenario $\bar{\mu}_l = \bar{a}_x$ & $\bar{a}_{y,\text{cst}}^- = 12.5$ & 6.5 m s^{-2} . The horizontal red dashed line indicates the maximum available electric machine acceleration $\bar{a}_{x,m} = \frac{F_{\text{max}}}{m_v}$. From this diagram we see that the vehicle operates at the limits of the given acceleration constraints in both scenarios. This means the mpSQP leverages the maximum acceleration potential in combination with fully available cornering potential.

D. Solver comparison

The number of variables in the performance profile within one QP for the performance trajectory is 126, including 810 constraints. From the problem formulation (34), a small number of non-zero entries in the matrices \mathbf{A} and \mathbf{P} of 2295 in total arises with constant entries in the problem's Hessian \mathbf{P} .

Fig. 10 contains a comparison of the ADMM solver OSQP [11] and the active set solver qpOASES [35] as QP solvers for an mpSQP method as proposed in this paper. Furthermore, we solve the original NLP using the interior point solver IPOPT [28] interfaced via CasADi [36] to obtain a measure of solution quality for the proposed mpSQP. Note that IPOPT is widely used to benchmark the solution quality even if it is not specifically designed for embedded optimization. We chose a scenario where the vehicle is heading towards a narrow right-hand turn at a high velocity of almost 200 km h^{-1} . The optimization horizon spans this turn including the consecutive straight where positive acceleration occurs. Therefore, the solvers have to deal with high gradients for the longitudinal force $F_x(s_m)$ and lateral acceleration $a_y(s_m)$ stemming from curve entry and exit. The velocity plot shows that the optimal solution z^* almost equals the initial guess z_{ini} for both the

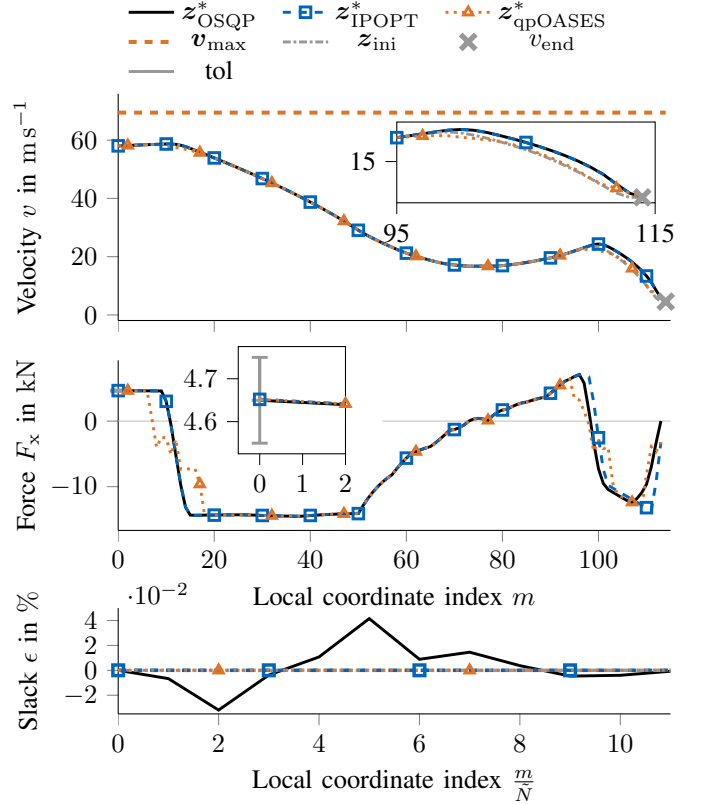


Fig. 10. Comparison of the solution of the mpSQP (internal QPs solved by the ADMM solver OSQP [11]) with the general NLP interior point solver IPOPT [28] interfaced by CasADi [36] and the active set solver qpOASES [35]. The chosen scenario includes the vehicle heading towards a narrow right-hand bend at a high velocity of almost 200 km h^{-1} . The optimization horizon spans the curve, and includes the subsequent straight.

velocity vector v and the slack values ϵ . This behavior is expected, as the previous SQP solution $z^{l-1}(s_m)$ is shifted by the traveled distance and used as initialization z_{ini} . The optimization outputs z^*_{OSQP} and z^*_{IPOPT} overlap except at the end of the planning horizon where IPOPT initially allows more positive longitudinal force $F_x(s_m)$, resulting in more aggressive braking to fulfill the hard constraint v_{end} . qpOASES's solution oscillates in the force $F_x(s_m)$ at the steep gradients. All the algorithms keep the initially given longitudinal force $F_x(s_s)$ within the specified tolerance of $\pm 0.1 \text{ kN}$, with OSQP matching the exact value (see magnified section in the second plot). The slack values ϵ are close to zero. However, the OSQP-solution shows small numerical oscillations within a negligible range of approx. $\pm 0.04\%$. Nevertheless this behavior is typical for an ADMM algorithm, and is thus noteworthy.

Apart from the solution qualities, we further analyzed the velocity optimization runtimes. The scenario consisted of two race laps, including a race start and coming to a standstill after the second lap on the Monteblando (Spain) race circuit with a variable acceleration potential along the circuit, cf. Subsection IV-C. The histograms in Fig. 11 display the calculation times Δt_{sol} for the number of calls C to optimize a speed profile. C_P and C_E denote the calls for the performance and the emergency lines, respectively. Their mean values are given

TABLE II
SOLVER MEAN RUNTIMES.

| CPU | Intel i7-7820HQ | | A57 ARM | |
|-------------------|-----------------|-------|---------|-------|
| | mpSQP | NLP | mpSQP | mpSQP |
| Prob. formulation | mpSQP | NLP | mpSQP | mpSQP |
| Solver | OSQP | IPOPT | qpOASES | OSQP |
| Performance in ms | 6.20 | 40.4 | 164 | 32.4 |
| Emergency in ms | 6.95 | 29.8 | 26.1 | 34.2 |

by $\Delta \tilde{t}_{\text{sol}}$. We wish to point out that the algorithm runtimes shown refer to an entire SQP optimization process for a speed profile consisting of the solution of several QPs in the case of the used solvers OSQP or qpOASES, which have been warm-started. The optimization runtimes on the specific CPUs are also summarized in Table II where the ARM A57 is the NVIDIA Drive PX2 CPU. As we selected OSQP for our application on the target hardware, we do not show additional solver times of IPOPT or qpOASES for the ARM A57 CPU.

Our mpSQP in combination with the QP solver OSQP reaches nearly equal mean runtimes of 6 ms to 7 ms for both velocity profiles on an Intel i7-7820HQ CPU and 32 ms to 34 ms on an A57 ARM CPU. An amount of 2 to 5 SQP iterations for the performance line was sufficient to reach the defined tolerances ε_{SQP} . To optimize the emergency speed profile, a higher amount of SQP iterations in the range of 5 - 10 was necessary. Therefore, the computational effort for the iterative linearizations increased on this profile. In contrast, it was possible to solve the single QPs in less calculation time, as less than half the number of optimization variables $M + N$ in comparison to the performance profile are present. With maximum computation times of 16.9 ms (73.3 ms A57 ARM) on the performance profile and 15.0 ms (77.1 ms A57 ARM) for the emergency line, we managed to stay far below our predefined process-timeouts, see Table I.

The same optimization problem was formulated with the CasADi-language [36] as a general NLP and passed to the interior point solver IPOPT. The IPOPT mean solver runtimes are at least approximately five times higher, with maxima of around 0.1 s on the emergency line being too long for vehicle operations at velocities beyond 200 km h⁻¹. On the emergency profile, the active set solver qpOASES beats IPOPT slightly in terms of its mean runtime $\Delta \tilde{t}_{\text{sol}}$ but consumes four times the IPOPT computation time to generate the performance speed profile, see Table II. This behavior is rational, as a higher number of optimization variables and active constraints increases the calculation speed of an active set solver significantly. Nevertheless, maximum computation times for the mpSQP of around 0.5 s on the performance line exclude the QP solver qpOASES for this type of application.

V. CONCLUSION

In this paper we presented a tailored mpSQP algorithm capable of adaptive velocity planning in real time for race cars operating at the limits of handling, and velocities above 200 km h⁻¹. The planner can deal with performance and emergency velocity profiles. Furthermore, the optimization handles multi-parametric input, e.g., from the friction estimation module or the race ES. We also specified the boundaries

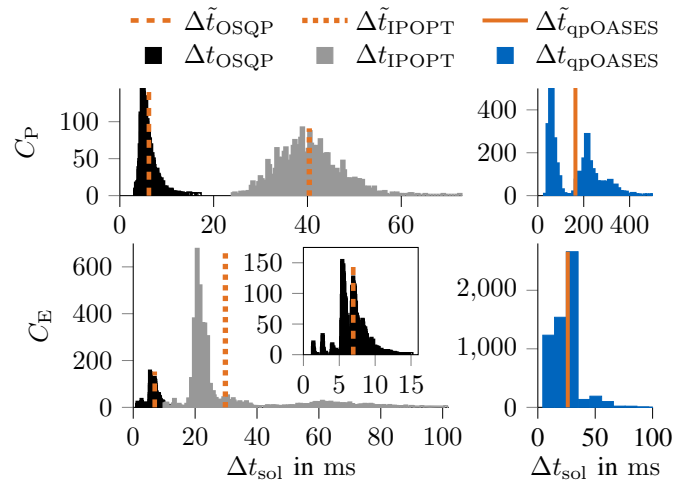


Fig. 11. Solver runtimes for the mpSQP with the local QPs solved by OSQP [11] or by the active set solver qpOASES [35], compared to the problem solved by the general NLP formulation passed to the interior point solver IPOPT interfaced by CasADi [36].

of maximum variation within these parameters to keep the problem feasible. Additionally, we compared different solvers applied to our problem formulation to compare calculation times as well as the solution qualities. Here, our mpSQP in combination with the ADMM solver OSQP outperformed the active set strategy qpOASES and the general NLP solver IPOPT in terms of calculation time, but reached nearly the same solution quality as IPOPT. This indicates that the first order ADMM in OSQP shows its strength for the minimum-time optimization problem as it handles the large set of active constraints well.

In future work we will apply the presented algorithm in autonomous races and implement a tailored trajectory optimization module based on the presented results and techniques for comparison.

CONTRIBUTIONS & ACKNOWLEDGMENTS

T. H. initiated the idea of the paper and contributed significantly to the concept, modeling, implementation and results. A. W. contributed to the design and feasibility analysis of the optimization problem. L. H. contributed essentially to the integration of variable acceleration limits. J. B. contributed to the whole concept of the paper. M. L. provided a significant contribution to the concept of the research project. He revised the paper critically for important intellectual content. M. L. gave final approval for the publication of this version and is in agreement with all aspects of the work. As a guarantor, he accepts responsibility for the overall integrity of this paper.

We would like to thank the Roborace team for giving us the opportunity to work with them and for the use of their vehicles for our research project. We would also like to thank the Bavarian Research Foundation (Bayerische Forschungsförderung) for funding us in connection with the “rAIcing” research project. This work was also conducted with basic research fund of the Institute of Automotive Technology from the Technical University of Munich.

REFERENCES

- [1] Chair of Automotive Technology, "Autonomous Driving Control Software of TUM Roborace," 2020. [Online]. Available: <https://github.com/TUMFTM>
- [2] —, "Python Package: Velocity Optimization," 2020. [Online]. Available: <https://pypi.org/project/velocity-optimization/>
- [3] M. Morari, F. Allgöwer, L. Magni, D. M. Raimondo, and M. Thoma, *Nonlinear Model Predictive Control: Towards New Challenging Applications*, ser. Lecture Notes in Control and Information Sciences. Berlin, Heidelberg: Springer Berlin Heidelberg, 2009, vol. 384.
- [4] T. Stahl, A. Wischnewski, J. Betz, and M. Lienkamp, "Multilayer Graph-Based Trajectory Planning for Race Vehicles in Dynamic Scenarios," in *2019 IEEE Intelligent Transportation Systems Conference (ITSC)*. IEEE, pp. 3149–3154.
- [5] A. Heilmeyer, A. Wischnewski, L. Hermansdorfer, J. Betz, M. Lienkamp, and B. Lohmann, "Minimum curvature trajectory planning and control for an autonomous race car," *Vehicle System Dynamics*, vol. 25, no. 8, pp. 1–31, 2019.
- [6] J. Betz, A. Wischnewski, A. Heilmeyer, F. Nobis, L. Hermansdorfer, T. Stahl, T. Herrmann, and M. Lienkamp, "A Software Architecture for the Dynamic Path Planning of an Autonomous Racecar at the Limits of Handling," in *2019 IEEE International Conference on Connected Vehicles and Expo (ICCVE)*. IEEE, 2019, pp. 1–8.
- [7] L. Hermansdorfer, J. Betz, and M. Lienkamp, "A Concept for Estimation and Prediction of the Tire-Road Friction Potential for an Autonomous Racecar," in *2019 IEEE Intelligent Transportation Systems Conference (ITSC)*. IEEE, pp. 1490–1495.
- [8] T. Herrmann, F. Passigato, J. Betz, and M. Lienkamp, "Minimum Race-Time Control-Strategy for an Autonomous Electric Racecar," in *2020 IEEE Intelligent Transportation Systems Conference (ITSC)*. IEEE, 2020 (In Press).
- [9] E. Ozatay, U. Ozguner, and D. Filev, "Velocity profile optimization of on road vehicles: Pontryagin's Maximum Principle based approach," *Control Engineering Practice*, vol. 61, pp. 244–254, 2017.
- [10] A. Liniger, A. Domahidi, and M. Morari, "Optimization-based autonomous racing of 1:43 scale RC cars," *Optimal Control Applications and Methods*, vol. 36, no. 5, pp. 628–647, 2015.
- [11] B. Stellato, G. Banjac, P. Goulart, A. Bemporad, and S. Boyd, "OSQP: an operator splitting solver for quadratic programs," *Mathematical Programming Computation*, vol. 5, no. 1, p. 42, 2020.
- [12] J. Betz, A. Wischnewski, A. Heilmeyer, F. Nobis, T. Stahl, L. Hermansdorfer, B. Lohmann, and M. Lienkamp, "What can we learn from autonomous level-5 motorsport?" in *9th International Munich Chassis Symposium 2018*, ser. Proceedings, P. Pfeffer, Ed. Wiesbaden: Springer Fachmedien Wiesbaden, 2019, pp. 123–146.
- [13] S. Ebbesen, M. Salazar, P. Elbert, C. Bussi, and C. H. Onder, "Time-optimal Control Strategies for a Hybrid Electric Race Car," *IEEE Transactions on Control Systems Technology*, vol. 26, no. 1, pp. 233–247, 2018.
- [14] D. J. N. Limebeer and G. Perantoni, "Optimal Control of a Formula One Car on a Three-Dimensional Track—Part 2: Optimal Control," *Journal of Dynamic Systems, Measurement, and Control*, vol. 137, no. 5, p. 051019, 2015.
- [15] A. J. Tremlett and D. J. N. Limebeer, "Optimal tyre usage for a Formula One car," *Vehicle System Dynamics*, vol. 54, no. 10, pp. 1448–1473, 2016.
- [16] F. Christ, A. Wischnewski, A. Heilmeyer, and B. Lohmann, "Time-optimal trajectory planning for a race car considering variable tyre-road friction coefficients," *Vehicle System Dynamics*, vol. 3, no. 1, pp. 1–25, 2019.
- [17] N. Dal Bianco, R. Lot, and M. Gadola, "Minimum time optimal control simulation of a GP2 race car," *Proceedings of the Institution of Mechanical Engineers, Part D: Journal of Automobile Engineering*, vol. 232, no. 9, pp. 1180–1195, 2018.
- [18] Y. Huang, H. Ding, Y. Zhang, H. Wang, D. Cao, N. Xu, and C. Hu, "A Motion Planning and Tracking Framework for Autonomous Vehicles Based on Artificial Potential Field Elaborated Resistance Network Approach," *IEEE Transactions on Industrial Electronics*, vol. 67, no. 2, pp. 1376–1386, 2020.
- [19] Y. Meng, Y. Wu, Q. Gu, and L. Liu, "A Decoupled Trajectory Planning Framework Based on the Integration of Lattice Searching and Convex Optimization," *IEEE Access*, vol. 7, pp. 130 530–130 551, 2019.
- [20] Y. Zhang, H. Chen, S. L. Waslander, J. Gong, G. Xiong, T. Yang, and K. Liu, "Hybrid Trajectory Planning for Autonomous Driving in Highly Constrained Environments," *IEEE Access*, vol. 6, pp. 32 800–32 819, 2018.
- [21] J. K. Subosits and J. C. Gerdes, "From the Racetrack to the Road: Real-Time Trajectory Replanning for Autonomous Driving," *IEEE Transactions on Intelligent Vehicles*, vol. 4, no. 2, pp. 309–320, 2019.
- [22] L. Svensson, M. Bujarbaruah, N. R. Kapania, and M. Torngren, "Adaptive Trajectory Planning and optimization at Limits of Handling," in *2019 IEEE/RSJ International Conference on Intelligent Robots and Systems (IROS)*. IEEE, pp. 3942–3948.
- [23] T. Mercy, R. van Parys, and G. Pipeleers, "Spline-Based Motion Planning for Autonomous Guided Vehicles in a Dynamic Environment," *IEEE Transactions on Control Systems Technology*, vol. 26, no. 6, pp. 2182–2189, 2018.
- [24] A. Carvalho, Y. Gao, A. Gray, E. Tseng, and F. Borrelli, "Predictive Control of an Autonomous Ground Vehicle using an Iterative Linearization Approach," in *16th International IEEE Conference on Intelligent Transportation Systems (ITSC), 2013*. Piscataway, NJ: IEEE, 2013.
- [25] B. Alrifae and J. Maczajewski, "Real-time Trajectory Optimization for Autonomous Vehicle Racing using Sequential Linearization," in *2018 IEEE Intelligent Transportation Systems Conference*. Piscataway, NJ: IEEE, 2018, pp. 476–483.
- [26] G. Williams, P. Drews, B. Goldfain, J. M. Rehg, and E. A. Theodorou, "Aggressive driving with model predictive path integral control," in *2016 IEEE International Conference on Robotics and Automation (ICRA)*. IEEE, 2016, pp. 1433–1440.
- [27] E. Alcalá, V. Puig, J. Quevedo, and U. Rosolia, "Autonomous racing using Linear Parameter Varying-Model Predictive Control (LPV-MPC)," *Control Engineering Practice*, vol. 95, p. 104270, 2020.
- [28] A. Wächter and L. T. Biegler, "On the implementation of an interior-point filter line-search algorithm for large-scale nonlinear programming," *Mathematical Programming*, vol. 106, no. 1, pp. 25–57, 2006.
- [29] L. Svensson, L. Masson, N. Mohan, E. Ward, A. P. Brenden, L. Feng, and M. Torngren, "Safe Stop Trajectory Planning for Highly Automated Vehicles: An Optimal Control Problem Formulation," in *2018 IEEE Intelligent Vehicles Symposium (IV)*. IEEE, 2018, pp. 517–522.
- [30] B. Houska, H. J. Ferreau, and M. Diehl, "ACADO toolkit-An open-source framework for automatic control and dynamic optimization," *Optimal Control Applications and Methods*, vol. 32, no. 3, pp. 298–312, 2011.
- [31] T. Lipp and S. Boyd, "Minimum-time speed optimisation over a fixed path," *International Journal of Control*, vol. 87, no. 6, pp. 1297–1311, 2014.
- [32] T. Denton, *Automated Driving and Driver Assistance Systems*, first edition ed. Abingdon, Oxon and New York, NY: Routledge, 2020.
- [33] G. Banjac, P. Goulart, B. Stellato, and S. Boyd, "Infeasibility Detection in the Alternating Direction Method of Multipliers for Convex Optimization," *Journal of Optimization Theory and Applications*, vol. 183, no. 2, pp. 490–519, 2019.
- [34] T. Herrmann, F. Christ, J. Betz, and M. Lienkamp, "Energy Management Strategy for an Autonomous Electric Racecar using Optimal Control," in *2019 IEEE Intelligent Transportation Systems Conference (ITSC)*. IEEE, pp. 720–725.
- [35] H. J. Ferreau, C. Kirches, A. Potschka, H. G. Bock, and M. Diehl, "qpOASES: a parametric active-set algorithm for quadratic programming," *Mathematical Programming Computation*, vol. 6, no. 4, pp. 327–363, 2014.
- [36] J. A. E. Andersson, J. Gillis, G. Horn, J. B. Rawlings, and M. Diehl, "CasADi: a software framework for nonlinear optimization and optimal control," *Mathematical Programming Computation*, vol. 11, no. 1, pp. 1–36, 2019.
- [37] D. G. Luenberger and Y. Ye, *Linear and Nonlinear Programming*, third edition ed., ser. International Series in Operations Research & Management Science. New York, NY and Berlin and Heidelberg: Springer, 2008, vol. 116.
- [38] S. P. Boyd and L. Vandenberghe, *Convex optimization*, ser. Safari Tech Books Online. Cambridge, UK and New York: Cambridge University Press, 2004.
- [39] P. T. Boggs and J. W. Tolle, "Sequential Quadratic Programming," *Acta Numerica*, vol. 4, pp. 1–51, 1995.
- [40] J. Nocedal and S. J. Wright, *Numerical Optimization*, second edition ed., ser. Springer Series in Operations Research and Financial Engineering. New York, NY: Springer Science+Business Media LLC, 2006.
- [41] F. Braghin, F. Cheli, S. Melzi, and E. Sabbioni, "Race driver model," *Computers & Structures*, vol. 86, no. 13-14, pp. 1503–1516, 2008.
- [42] E. C. Kerrigan, "Soft Constraints and Exact Penalty Functions in Model Predictive Control," in *Proceedings of the United Kingdom Automatic Control Council 2000*, IFAC, Ed., 2000.



Thomas Herrmann was awarded a B.Sc. and an M.Sc. in Mechanical Engineering by the Technical University of Munich (TUM), Germany, in 2016 and 2018, respectively. He is currently pursuing his doctoral studies at the Institute of Automotive Technology at TUM where he is working as a Research Associate. His current research interests include optimal control in the field of trajectory planning for autonomous vehicles and the efficient incorporation of the electric powertrain behavior within these optimization problems.



Alexander Wischnewski was awarded a B.Eng. in Mechatronics by the DHBW Stuttgart in 2015, and an M.Sc. in Electrical Engineering and Information Technology by the University of Duisburg-Essen, Germany, in 2017. He is currently pursuing his doctoral studies at the Chair of Automatic Control at the Department of Mechanical Engineering at Technical University of Munich (TUM), Germany. His research interests lie at the intersection of control engineering and machine learning, with a strong focus on autonomous driving.



Leonhard Hermansdorfer was awarded a B.Sc. and an M.Sc. in Mechanical Engineering by the Technical University of Munich (TUM), Germany, in 2015 and 2018, respectively. He is currently pursuing his doctoral studies at the Institute of Automotive Technology at TUM where he is working as a Research Associate. His current research interest is the identification of a vehicle's maximum transmittable tire forces, with a strong focus on model-less approaches based on machine learning.



Johannes Betz is currently a postdoctoral researcher at the Technical University of Munich (TUM). He graduated in 2013 with an M.Sc. in Automotive Technology from the University of Bayreuth, Germany. He graduated with a doctoral degree from TUM about the topic of fleet disposition for electric vehicles. Since then, he continues his research in the field of autonomous driving. His research topics include the dynamic trajectory and behavioral planning for autonomous vehicles at the handling limits, as well as prediction of traffic participant behavior

in non-deterministic environments.



Markus Lienkamp studied Mechanical Engineering at TU Darmstadt, Germany, and Cornell University, USA, and received a Ph.D. degree from TU Darmstadt in 1995. He was with Volkswagen as part of an International Trainee Program and took part in a joint venture between Ford and Volkswagen in Portugal. Returning to Germany, he led the Brake Testing Department, VW Commercial Vehicle Development Section, Wolfsburg. He later became the Head of the "Electronics and Vehicle" Research Department, Volkswagen AG's Group Research Division.

His main priorities were advanced driver assistance systems and vehicle concepts for electromobility. He has been Head and Professor of the Institute of Automotive Technology, Technical University of Munich (TUM), Germany, since November 2009. He is conducting research in the area of electromobility, autonomous driving and mobility.